Impact of pure dephasing on the nonlinear optical response of single quantum dots and dot ensembles

A. Vagov, V. M. Axt, and T. Kuhn
Institut für Festkörpertheorie, Westfälische-Wilhelms Universität, Wilhelm-Klemm-Strasse 10, 48149 Münster, Germany
(Received 6 December 2002; published 28 March 2003)

The nonlinear optical response to ultrafast laser pulses of semiconductor quantum dots coupled to acoustic phonons is discussed on the basis of closed-form analytical results valid for dots in the strong confinement regime. General properties of four-wave-mixing (FWM) signals are derived from the analytical formulas. Numerical results are presented for two-pulse FWM signals from single quantum dots and from dot ensembles in the time and the frequency domains. Interestingly, the initial decay time of the signal is found to depend nonmonotonously on temperature and delay time. In general, the phonon coupling leads to a modulated decay of the time domain optical response which is neither exponential nor Gaussian. The strength of the modulations is influenced by inhomogeneous broadening and temperature as well as by the relative localization lengths of electrons and holes. FWM spectra of single dots evolve from asymmetric functions for coinciding pulses into symmetric spectra for large delays. Nonlinear signals are compared with linear signals revealing striking similarities but also significant differences, e.g., concerning the depth of the initial drop.

DOI: 10.1103/PhysRevB.67.115338 PACS number(s): 78.67.Hc, 78.47.+p, 63.20.Kr, 63.22.+m

I. INTRODUCTION

The analysis of coherent nonlinear optical signals emitted after ultrafast laser excitation has contributed considerably to our present understanding of wide classes of materials. With regard to semiconductor quantum dots, however, such experiments are bothered by rather low signal intensities. Despite these difficulties, there are a number of recent reports on experiments demonstrating the manipulation of quantum dots by coherent optical laser pulses.[1–7] Particularly promising in view of potential applications of quantum dots for quantum information processing[8–16] is the growing number of demonstrations of Rabi rotations under varying experimental conditions.[17–22] Coherent nonlinear optical measurements also gave valuable insight into the decoherence properties of quantum dots which are of prime importance for any optoelectronic device and especially for realizations of quantum computational operations. In particular, four-wave-mixing (FWM) experiments[3,23–26] and measurements of three-pulse photon echos[7] or accumulated photon echos[27,28] have been most useful for the quantification of the optical decoherence of quantum dots. For some systems ultralong dephasing times of the order of hundreds of picoseconds have been reported.[3,26] Prior to such a slow long-time decay a rather rapid initial decay is observed typically on a picosecond timescale, which leads to a significant drop of the signal at elevated temperatures. It has been concluded from a number of experimental and theoretical studies that in quantum dots the so-called *pure dephasing* induced by the carrier-phonon coupling is a major source for this initial optical decoherence.[29–33] Pure dephasing refers to the decoherence caused by those parts of the electron-phonon coupling that do not change the electronic occupation numbers. For higher-dimensional systems these parts yield only small corrections to *real* phonon transitions which lead to electronic redistributions and thus to energy relaxation. However, real transitions are strongly suppressed in quantum dots due to the discrete electronic energy structure, a phenomenon commonly refered to as a *phonon bottleneck*.[34,35] Although there is considerable theoretical work related to coupled dot-phonon systems[29,32,36–44] little is known about the nonlinear optical response of such systems. In particular, with respect to dephasing most studies concentrated on estimations of the resulting linewidth[29,32,36,37] or the determination of line shapes of linear absorption[33] or emission[30] spectra.

In the present paper we discuss in detail the effects of pure dephasing on FWM signals emitted from single quantum dots as well as from dot ensembles. Our analysis is based on a theoretical approach which formulates the dynamics of the coupled carrier-phonon system in terms of generating functions for phonon-assisted density matrices.[33,45–47] By using this formalism we have recently been able to derive in closed form the nonlinear optical response to an arbitrary sequence of ultrafast laser pulses of dots with strongly confined carriers coupled to an arbitrary number of phonon modes.[48] It is worth noting that within our model the results are nonperturbative with respect to both the carrier-phonon coupling as well as the carrier-light coupling. Furthermore, the general form of the solution has been derived without making any assumptions about the phonon dispersion, the wave-vector dependence of the carrier-phonon coupling, or the form of the carrier wave functions. In order to illustrate typical properties of the nonlinear optical response predicted by our general formulas we consider in the present paper a prototype model for a spherical GaAs quantum dot coupled to bulk acoustic phonons via the deformation potential. Using this model we calculate time and frequency domain two-pulse FWM signals emitted from single dots as well as from dot ensembles. We analyze the resulting line shapes for varying temperatures, delay times, and localization lengths of electrons and holes.

FWM experiments are often used to extract homogeneous lifetimes, which in linear experiments are masked by inhomogeneous broadening. Therefore, it is also of interest to discuss in detail the relation between the linear response of a

 ©2003 The American Physical Society

single dot which is representative for an exclusively homogeneously broadened system and FWM signals emitted from dot ensembles. Here, we consider an ensemble of dots with varying sizes and discuss the effects caused by the corresponding fluctuations of the carrier-phonon couplings and the electronic energies.

Many features of our numerical results can be related to analytical properties of the closed-form solution. A discussion of these properties reveals that in most cases the qualitative behavior can be derived without knowing details of the electronic wave functions. These properties are therefore generic features which do not depend on the simplifying assumptions made in our specific numerical implementation.

The paper is organized as follows: we start in Sec. II by defining our model. In Sec. III we then relate the general solution of Ref. 48 to our specific situation and give explicit formulas for all signals of interest that are discussed in the present paper. In Secs. IV A and IV B we analytically establish a number of general properties of our solution in the time and frequency domains. This analysis is continued in Sec. IV C where we relate features of the optical response to some basic properties of the form factor for the carrier-phonon coupling. The remaining sections are devoted to numerical investigations. We start in Sec. V A by analyzing FWM signals from single quantum dots. In Sec. V B the discussion is extended to dot ensembles. Here, a detailed comparison with the linear response from a single dot is also included. Section V C deals with a specific feature of our solution, namely, that even a smooth continuum of acoustic phonons will in general lead to nonmonotonous modulations of the time domain response. Finally, we present concluding remarks.

II. MODEL

For semiconductor quantum dots in the limit of strong electronic confinement it is justified to concentrate on only two electronic states representing the uppermost valence and the lowest conduction-band state, respectively. In this case, the pertinent Hamiltonian for the analysis of phonon-induced pure dephasing can be written as[33,48]

$$H=\hbar\Omega c^{\dagger}c-(MEc^{\dagger}d^{\dagger}+M^{*}E^{*}dc)+\sum_{\xi}\hbar\omega_{\xi}b_{\xi}^{\dagger}b_{\xi}+\sum_{\xi}\hbar[(g_{\xi}^{e}b_{\xi}+g_{\xi}^{e*}b_{\xi}^{\dagger})c^{\dagger}c-(g_{\xi}^{h}b_{\xi}+g_{\xi}^{h*}b_{\xi}^{\dagger})d^{\dagger}d], \tag{1}$$

where c, d, and b_{ξ} are the annihilation operators for electrons, holes, and phonons, respectively; $c^{\dagger}$, $d^{\dagger}$, and $b_{\xi}^{\dagger}$ are the corresponding creation operators; and $g_{\xi}^{e,h}$ are phonon coupling constants. Here, the index ξ is used to label the phonon modes and $\hbar\omega_{\xi}$ are the corresponding phonon energies. M is the component of the dipole moment in the direction of the laser field polarization and $E(t)$ denotes the amplitude of the laser field. Finally, Ω is the energy of an electron occupying a conduction-band state confined to the dot. The energy of the uppermost hole state is taken as the zero of energy.

Obviously, the model contains two well-known limiting cases: when the electron-phonon coupling is disregarded, the Hamiltonian generating the *optical Bloch equations*[49] is recovered; if on the other hand the carrier-light-field coupling is absent then the so-called *independent boson model* is approached,[50] which has also been extensively studied.[50–53] In order to treat the carrier-phonon as well as the carrier-light interactions nonperturbatively three generating functions for phonon-assisted density matrices have been introduced in Ref. 33:

$$Y(\alpha_{\xi},\beta_{\xi},t)=\langle dce^{\Sigma_{\xi}\alpha_{\xi}b_{\xi}^{\dagger}}e^{\Sigma_{\xi}\beta_{\xi}b_{\xi}}\rangle,$$

$$C(\alpha_{\xi},\beta_{\xi},t)=\langle c^{\dagger}ce^{\Sigma_{\xi}\alpha_{\xi}b_{\xi}^{\dagger}}e^{\Sigma_{\xi}\beta_{\xi}b_{\xi}}\rangle,$$

$$F(\alpha_{\xi},\beta_{\xi},t)=\langle e^{\Sigma_{\xi}\alpha_{\xi}b_{\xi}^{\dagger}}e^{\Sigma_{\xi}\beta_{\xi}b_{\xi}}\rangle,$$

where α_{ξ} and β_{ξ} are complex valued parameters and the brackets denote the quantum-mechanical averaging over electron and phonon degrees of freedom. All components of the electronic and phononic density matrices and all electron-phonon correlation functions can be obtained from the values of the functions Y, C, and F at $\alpha_{\xi}=\beta_{\xi}=0$ or from their derivatives with respect to α_{ξ},β_{ξ} taken at this point.

The dynamics defined by the model Eq. (1) is completely determined by the time evolution of these generating functions which is governed by a closed set of coupled partial differential equations. General nonperturbative analytical solutions for the dymamics of Y, C, and F have been obtained for the important case of an excitation by an arbitrary sequence of deltalike light pulses.[48] In the derivation of these solutions no assumptions have been made about the form of the phonon coupling constants $g_{\xi}^{e(h)}$, the phonon dispersion ω_{ξ}, or the electron and hole wave functions. In the present paper we use a model relevant for a prototype GaAs quantum dot coupled to bulk phonons. For such a system it has been found in Ref. 33 that the deformation potential coupling to longitudinal-acoustic (LA) phonons has the strongest impact on the optical properties, in particular on the decoherence. Therefore, it is justified to concentrate here exclusively on this mechanism and label the phonons from now on by their wave vector q. The corresponding carrier-phonon coupling constants are then given by

$$g_{q}^{e(h)}=\Psi^{e(h)}(\mathbf{q})\frac{qD^{e(h)}}{\sqrt{2V\rho\hbar\omega_{q}}}, \tag{2}$$

where ρ is the density of the material, ω_{q} is the acoustic-phonon dispersion, V is the normalization volume, and $D^{e(h)}$ is the deformation-potential constant for electrons (holes). Finally, we have to specify the wave functions for electrons and holes which determine the carrier form factor $\Psi^{e(h)}(\mathbf{q})$. For simplicity we use the same spherical dot model that has been applied for calculations in Ref. 48, resulting in a carrier form factor given by

$$\Psi^{e(h)}(\mathbf{q}) = \exp\left[-\frac{q^2 a_{e(h)}^2}{4}\right], \tag{3}$$

where $a_{e(h)}$ is the localization length of the trapped electron (hole). Unless otherwise stated we set $a_e = 4$ nm and use a localization ratio $r = a_h/a_e = 0.87$. This ratio corresponds to the assumption that the confinement potentials have the same shape for electrons and holes. The ratio r then follows from the mass ratio.[33]

III. FWM SIGNALS FROM A SINGLE DOT AND DOT ENSEMBLES

FWM signals are important manifestions of the coherent nonlinear optical response of the system. Unlike signals from higher-dimensional semiconductor systems, coherent signals from a single quantum dot are usually not selectively emitted in a phase-matching direction. A FWM signal from a dot is therefore not related to a corresponding direction selection of the emitted signal. Typical experiments use heterodyne detection techniques,[3,25] which by means of suitable low-frequency modulations essentially filter out the component P_{FWM} of the nonlinear polarization that depends on the phases φ_1 and φ_2 of the two exciting pulses as $e^{i(2\varphi_2-\varphi_1)}$. It is worth noting that the measured signal is proportional to the *amplitude* $|P_{\mathrm{FWM}}|$ due to the heterodyne detection.

Theoretically, any component of the linear or nonlinear optical response is determined by the polarization P which is related to the transition density Y by

$$P(t) = M^* Y(\alpha_q, \beta_q, t)\big|_{\alpha_q=\beta_q=0}. \tag{4}$$

In particular, the degenerate FWM signal can be extracted from the polarization P, created by two consecutive light pulses arriving at times $t_1 = -\tau$ and $t_2 = 0$. Within our model the exact result for two delta-shaped pulses has been derived in Ref. 48. It reads

$$P_{\mathrm{FWM}}(t,\tau) = -\frac{i}{2}\Theta(t)\Theta(\tau)M^*\sin^2\left(\frac{f_2}{2}\right)\sin(f_1) \times e^{i(2\varphi_2-\varphi_1)}e^{-i\bar{\Omega}(t-\tau)}G_{\mathrm{FWM}}(t,\tau), \tag{5}$$

where $f_{1,2}$ are the pulse areas of the two light pulses, and the envelope function $G_{\mathrm{FWM}}(t,\tau)$ is given by

$$G_{\mathrm{FWM}}(t,\tau) = \exp\Bigg[\sum_q |\gamma_q|^2 (i\{2\sin(\omega_q\tau) - \sin[\omega_q(t+\tau)]\} - (1+2N_q)\{3 - 2\cos(\omega_q\tau) - 2\cos(\omega_q t) + \cos[\omega_q(t+\tau)]\})\Bigg]. \tag{6}$$

Here, $N_q = [\exp(\hbar\omega_q/k_B T) - 1]^{-1}$ denotes the Bose distribution of the phonons at temperature T and the theta function $\Theta(t)$ is 1 for $t > 0$ and 0 otherwise. Furthermore, we have used the abbreviations

$$\bar{\Omega} = \Omega - \sum_q |\gamma_q|^2 \omega_q, \quad \gamma_q = \frac{g_q^e - g_q^h}{\omega_q} \tag{7}$$

for the polaron shifted exciton frequency $\bar{\Omega}$ and the dimensionless phonon coupling γ_q. The factor $e^{-i\bar{\Omega}(t-\tau)}$ in Eq. (5) sets the overall scale for the free oscillations of the induced polarization, while all other information about the temporal behavior of the signal is contained in the dimensionless function $G_{\mathrm{FWM}}(t,\tau)$.

The expression Eq. (5) represents the FWM signal emitted from a single dot. Experiments, however, are much easier to perform on samples containing few thousands of dots. The main difference between such dot ensembles and a single dot is that the parameters that characterize the dots may strongly fluctuate, and a meaningful comparison with such experiments requires an ensemble averaging of Eq. (5). The effect of these fluctuations on the optical signal is commonly referred to as *inhomogeneous broadening*.

We will assume that there are no direct couplings between different dots in the ensemble and that the wave functions of all electrons and holes can be described by Gaussians. Then Eq. (5) represents the contribution of a given dot in the ensemble and the response of the ensemble is determined by averaging over the dot parameters. This leaves four potentially fluctuating dot parameters in the model: the energy of the excitonic state, Ω; the localization lengths, a_e and a_h; and the laser light coupling constant M. Fluctuations of M lead to a renormalization of the amplitude of the signal and when the signals are recorded as functions of the pulse intensities a damping of the Rabi oscillations is obtained, an effect that has been studied, e.g., in Refs. 20 and 21 and that will not be pursued here.

Little is known about the way in which the remaining parameters are distributed in typical ensembles. In this paper the analysis of ensemble-averaged signals is based on the following two assumptions: (i) the confinement potential is given by the same parabola for electrons and holes, resulting in a localization ratio r determined by the mass ratio. For GaAs parameters we thus have $r = 0.87$; (ii) the fluctuations of the energies are exclusively due to the dot-size-dependent changes of the confinement energies defined by the three-dimensional harmonic confinement potential, i.e., we assume that

$$\hbar\bar{\Omega} = \hbar\bar{\Omega}_0 + \hbar\bar{\Omega}(a_e) = \hbar\bar{\Omega}_0 + \frac{3}{2}\frac{\hbar^2}{a_e^2}\left(\frac{1}{m_e} + \frac{1}{r^2 m_h}\right), \tag{8}$$

where $\hbar\bar{\Omega}_0$ is not fluctuating from dot to dot. Using the above two assumptions, the fluctuations of the energies and the localization lengths a_e and a_h are correlated and can be parametrized by a single quantity. We will use the electron localization length a_e to uniquely characterize the different dots within the ensemble and assume a Gaussian distribution of a_e with mean value $\bar{a}_e$ and deviation σ_a. The ensemble-averaged polarization is obtained for this model by substituting in Eq. (5) the function

$$G_{\mathrm{FWM}}^{\mathrm{ens}}(t,\tau) := \int da_e G_{\mathrm{FWM}}(t,\tau) \times A_0 \exp\left[-\frac{(a_e-\bar{a}_e)^2}{2\sigma_a^2} - i\bar{\Omega}(a_e)(t-\tau)\right] \tag{9}$$

for $G_{\mathrm{FWM}}(t,\tau)$ and replacing the polaron shifted exciton frequency $\overline{\Omega}$, occurring in the factor $e^{-i\overline{\Omega}(t-\tau)}$, by the nonfluctuating part $\overline{\Omega}_0$. The factor A_0 in Eq. (9) ensures the normalization of the size distribution. Physically it is clear that dots of arbitrarily small sizes cannot exist. This implies that the integration in Eq. (9) must have a lower cutoff at a finite value $a_{\min}$. For all calculations we have set the cutoff to $a_{\min}=1$ nm and used a mean value of $\overline{a_e}=4$ nm. The localization ratio was kept at $r=0.87$.

It should be noted that in addition to the energy the factor $G_{\mathrm{FWM}}(t,\tau)$ is affected by the size fluctuations because the carrier wave functions and therefore the form factors in Eq. (3), which determine the strength of the carrier-phonon coupling, depend on the localization lengths a_e and a_h.

For large energy fluctuations the averaging over the oscillating factor $\exp[-i\overline{\Omega}(a_e)(t-\tau)]$ in Eq. (9) produces a sharp echo peak centered at $t=\tau$, which has also been observed in recent FWM experiments on dot ensembles.[3] While the occurrence of a sharp echo primarily reflects the presence of strong inhomogeneous broadening, the corresponding time integral still contains valuable information about the homogeneous decay.[54] In addition to the time resolved signals defined so far it is, therefore, also interesting to study the time-integrated response which is measured in many experiments. Usually, time-integrated amplitudes are recorded, which are determined by the functions

$$\tilde{G}^{\mathrm{ens}}_{\mathrm{FWM}}(\tau) := \int_0^\infty |G^{\mathrm{ens}}_{\mathrm{FWM}}(t,\tau)|\,dt. \tag{10}$$

To facilitate the comparison of the delay-time behavior of $\tilde{G}^{\mathrm{ens}}_{\mathrm{FWM}}(\tau)$ with the behavior of the dimensionless function $G_{\mathrm{FWM}}(t,\tau)$ it is convenient to normalize the former according to

$$\overline{G}^{\mathrm{ens}}_{\mathrm{FWM}}(\tau) := \tilde{G}^{\mathrm{ens}}_{\mathrm{FWM}}(\tau)/\tilde{G}^{\mathrm{ens}}_{\mathrm{FWM}}(\tau=0). \tag{11}$$

Besides the discussion of the above-defined signals it turns out to be instructive to compare nonlinear optical signals with the linear response. The latter is fully determined by the linear polarization induced by a single delta-shaped pulse. For a single dot excited by a delta pulse at $t_1=0$ it reads[33,48]

$$P_{\mathrm{lin}}(t)=\frac{i}{2}\Theta(t)M^* f_1 e^{i\varphi_1}e^{-i\overline{\Omega}t}G_{\mathrm{lin}}(t), \tag{12}$$

where

$$G_{\mathrm{lin}}(t)=\exp\Bigg(-\sum_q |\gamma_q|^2\{i\sin(\omega_q t) + (1+2N_q)[1-\cos(\omega_q t)]\}\Bigg). \tag{13}$$

First, we note that apart from constant prefactors the single dot FWM signal, Eq. (5), in the limit $\tau\to 0$ coincides with the linear signal, Eq. (12). Obviously, for other values of τ the envelope function $G_{\mathrm{lin}}(t)$ differs from its nonlinear counterpart. In order to get more insight into the relation between linear and nonlinear signals it is helpful to consider as a reference a model with phenomenological damping constants. In this case the time-integrated FWM amplitude of a system with infinitely strong inhomogeneous broadening would, apart from constant prefactors, exhibit the same temporal behavior as the absolute square of the linear polarization.[54] Of course, the time argument corresponds to the delay time in the former case and to the real time in the latter case. In both cases delta pulse excitation is assumed. Therefore, a meaningful comparison is obtained when $|G_{\mathrm{lin}}|^2$ is compared with a function $\overline{G}_\infty$ representing the FWM envelope of an ensemble with infinitely large energy fluctuations. For this comparison we will disregard the effects of fluctuations of the carrier-phonon coupling and concentrate exclusively on the energy fluctuations. It is clear that the limit of an *infinitely* broadened ensemble is an idealization which is expected to hold for a system with a finite broadening that is much larger than the typical spectral width of a single dot in the ensemble. We will come back to this point later when we discuss the transition from a finite to an infinite inhomogeneous broadening. In the latter case analytical results are much easier to obtain. In particular, the echo discussed above evolves into a delta peak when the broadening is large and, therefore, the evaluation of the time integral in Eq. (10) yields

$$\overline{G}_\infty(\tau)=|G_{\mathrm{FWM}}(\tau,\tau)|. \tag{14}$$

Using Eq. (6) we find explicitly

$$\overline{G}_\infty(\tau)=\exp\Bigg\{-2\sum_q |\gamma_q|^2(1+2N_q)[1-\cos(\omega_q\tau)]^2\Bigg\}. \tag{15}$$

Comparing Eq. (13) with Eq. (15) we find that the expression for $\overline{G}_\infty$ is related to $|G_{\mathrm{lin}}|^2$ by replacing the factor $[1-\cos(\omega_q t)]$ in the definition of $|G_{\mathrm{lin}}|^2$ by the term $[1-\cos(\omega_q\tau)]^2$.

IV. GENERAL PROPERTIES

The optical signals defined above possess a number of generic properties that can be observed for a broad class of models for the phonon coupling constants. With respect to these properties the numerical results presented below are, therefore, representative for a wide class of dot systems and are not restricted to the simplified model used in the specific evaluation. Some of these generic properties follow from asymptotic expansions of the corresponding analytical formulas and thus are observed for any choice of the coupling constants. Others are related to elementary features characterizing the form factor for a given dot structure. We consider the former first.

A. Asymptotic behavior

The FWM envelope $G_{\mathrm{FWM}}(t,\tau)$ for a single quantum dot defined in Eq. (6) is typically a decaying function of t provided that γ_q is a smooth function without singularities ex-

cept for a possible integrable singularity at $q=0$ and provided that the phonon spectrum ω_q is a smooth continuum. For acoustic phonons coupled by the deformation potential this is usually satisfied. Phonon bulk modes may be taken as a prototype for a typical dependence of γ_q and ω_q on the wave vector q. In this case the coupling is given by Eq. (2) and a linear dispersion can be used for all modes that are effectively coupled to the carriers. In the following we assume $\omega_q \approx cq$ for all relevant modes.

The real-time decay of $G_{\mathrm{FWM}}(t,\tau)$ confirms the earlier observation[33] that LA phonons destroy the optical coherence of the exciton. Indeed, despite the absence of phonon-mediated carrier level transitions a decay of both the linear polarization and the FWM signal is found. However, as explained in Ref. 33 it is the asymptotic behavior of $|\gamma_q|^2$ for vanishing q which determines whether or not the polarization decays to zero in the long-time limit. For an electrically neutral exciton, $|\gamma_q|^2$ is expected to have a singularity at $q=0$ not stronger than $|\gamma_q|^2 \propto 1/q$ and thus according to the considerations in Ref. 33 the polarization does not decay to zero in this case; instead a finite value is approached for $t\to\infty$. If there is no further singularity in $|\gamma_q|^2$ the corresponding limiting value of Eq. (6) can be derived according to the procedure outlined in the Appendix resulting in

$$G_{\mathrm{FWM}}(\infty,\tau)=\exp\left(\sum_q |\gamma_q|^2\{2i\sin(\omega_q\tau) - (1+2N_q)[3-2\cos(\omega_q\tau)]\}\right). \quad (16)$$

This is in general a decreasing function of temperature and typically it also decreases with increasing delay time. Expanding the Bose factor $(1+2N_q)$ in the high-temperature limit, i.e., $(1+2N_q)\approx 2k_BT/(\hbar cq)$, it is seen from Eq. (16) that the absolute value of $G_{\mathrm{FWM}}(\infty,\tau)$ decreases exponentially with temperature according to

$$|G_{\mathrm{FWM}}(\infty,\tau)| \overset{T\to\infty}{\to} \exp\left(-\frac{2k_BT}{\hbar c}\sum_q \frac{|\gamma_q|^2}{q}[3-2\cos(\omega_q\tau)]\right). \quad (17)$$

Equation (17) implies that the exponential temperature dependence of the limiting value of the optical response is a generic property which is found whenever the carrier-phonon couplings $|\gamma_q|^2$ are smooth continuous functions; only the value of the exponential decay constant is model dependent.

Similar to the $t\to\infty$ limit, Eq. (6) has a finite asymptotic value also in the limit $\tau\to\infty$. It is worthwhile to note that this value coincides with the absolute value of Eq. (16),

$$G_{\mathrm{FWM}}(t,\infty)=|G_{\mathrm{FWM}}(\infty,t)|. \quad (18)$$

Equation (18) reveals another interesting generic property: the FWM envelope of a single dot becomes real at large delay times.

Also the time-integrated FWM amplitude of an infinitely strong inhomogeneously broadened dot ensemble, Eq. (15), yields a finite value for $\tau\to\infty$ given by (cf. also the derivation in the Appendix)

$$\bar{G}_\infty(\tau\to\infty)=\exp\left(-3\sum_q |\gamma_q|^2(1+2N_q)\right), \quad (19)$$

which declines exponentially in the high-temperature limit as

$$\bar{G}_\infty(\tau\to\infty) \overset{T\to\infty}{\to} \exp\left(-\frac{6k_BT}{c\hbar}\sum_q \frac{|\gamma_q|^2}{q}\right). \quad (20)$$

As mentioned earlier, a dephasing model with phenomenological decay constants suggests that $\bar{G}_\infty$ should behave similarly to $|G_{\mathrm{lin}}|^2$. However, from Eq. (13) we find asymptotically for $t\to\infty$ that

$$|G_{\mathrm{lin}}(t\to\infty)|^2=\exp\left(-2\sum_q |\gamma_q|^2(1+2N_q)\right). \quad (21)$$

Comparing Eq. (21) with the corresponding result for $\bar{G}_\infty$ in Eq. (19) we conclude that using the linear response, Eq. (13), to estimate the behavior of the time-integrated FWM signal $\bar{G}_\infty$ (among other things) systematically overstates the limiting value of the signal amplitude, especially at large temperatures.

The temperature also affects the initial decay rate of the signal which is the characteristic time needed for the signal to approach its limiting value. In the limit of high temperatures the character of the corresponding temperature dependence is again independent of the phonon coupling model and can be obtained by using the high-temperature approximation for the Bose factor together with the expansion $\cos(\omega_q t)\approx 1-\omega_q^2 t^2/2$ which is valid for short times. For the amplitude $|G_{\mathrm{FWM}}(t,\tau=0)|$ we obtain in this way

$$|G_{\mathrm{FWM}}(t,0)|\propto \exp(-t^2 c\Gamma k_BT/\hbar), \Gamma=\sum_q q|\gamma_q|^2, \quad (22)$$

from which the temperature dependence of the initial decay time is extracted to be

$$t_0 \approx \sqrt{\frac{\hbar}{c\Gamma k_BT}}. \quad (23)$$

As expected, $t_0(T)$ declines monotonously for high temperatures. In contrast, the decay time of the signal at low temperatures turns out to depend on the parameters of the dot. By assuming an asymptotic behavior determined by the form factor in Eq. (3) it is possible to obtain an estimation[48] $t_0\approx t_{ph}=a/c$, where a is a characteristic length describing the spatial extension of the dot. Thus, the initial decay time should be determined by the time phonons need to leave the dot. More accurate estimations for t_0 require a detailed knowledge of the phonon coupling.

B. Spectra

Besides optical properties in the time domain we shall also explore the system response in the frequency domain. However, some care has to be taken in order to define meaningful spectra, because in our model the signals do not decay to zero for long times. It is therefore helpful to introduce the following decomposition:

$$G_{\mathrm{FWM}}(t,\tau)=G_{\mathrm{FWM}}(\infty,\tau)+\Delta G_{\mathrm{FWM}}(t,\tau). \tag{24}$$

The function $\Theta(t)\Delta G_{\mathrm{FWM}}(t,\tau)$ decays to zero in the long-time limit $t\to\infty$ and has a well-defined Fourier transform,

$$\Delta G_{\mathrm{FWM}}(\omega,\tau)=\int_0^\infty e^{i\omega t}\Delta G_{\mathrm{FWM}}(t,\tau)dt. \tag{25}$$

According to the decomposition, Eq. (24), the Fourier transform of $\Theta(t)G_{\mathrm{FWM}}(t,\tau)$ is the superposition of $\Delta G_{\mathrm{FWM}}(\omega,\tau)$ and a singular part $G_s(\omega,\tau)$,

$$G_{\mathrm{FWM}}(\omega,\tau)=G_s(\omega,\tau)+\Delta G_{\mathrm{FWM}}(\omega,\tau), \tag{26}$$

where the singular part is given by the Fourier transform of the step function $\Theta(t)G_{\mathrm{FWM}}(\infty,\tau)$ which results in the distribution

$$G_s(\omega,\tau):=\lim_{\delta\to 0^+}\frac{iG_{\mathrm{FWM}}(\infty,\tau)}{\omega+i\delta}. \tag{27}$$

Since the FWM polarization differs from $\Delta G_{\mathrm{FWM}}(t,\tau)$ only by the oscillating function $e^{-i\tilde{\Omega}(t-\tau)}$ and some constant prefactors, the polarization spectrum can be obtained from $G_{\mathrm{FWM}}(\omega,\tau)$ by a simple scaling and shifting of the resulting curves.

The singular part $G_s(\omega,\tau)$ is responsible for the sharp structure in the polarization spectrum which is commonly refered to as the *zero-phonon line*. According to Eq. (27) its weight is determined by the limiting value

$$W_s(\tau):=\left|G_{\mathrm{FWM}}(t\to\infty,\tau)\right|. \tag{28}$$

It is clear that interactions that have not yet been taken into account in our model such as the radiative decay will eventually lead to a vanishing signal in the long-time limit. Experimentally, several hundreds of picoseconds have been reported for low temperatures.[3,26] Of course, it would be easy to account phenomenologically for such a decay by assigning a finite value to δ in Eq. (27). However, the measurements show a significant temperature dependence of the decay constant for long times and it is, therefore, clear that radiative decay alone cannot account for the measured data. The microscopic origin of this long-time decay is still an open question which is not addressed in the present paper. We also make no attempts to include this feature on a phenomenological basis. Instead, we characterize the singular component of the spectra, Eq. (26), by its weight $W_s(\tau)$ and discuss separately the properties of the nonsingular part $\Delta G_{\mathrm{FWM}}(\omega,\tau)$. As we see below, the nonsingular part provides for a broad background on which the singular part has to be superimposed in order to obtain the full spectrum $G_{\mathrm{FWM}}(\omega,\tau)$. We will therefore also refer to $\Delta G_{\mathrm{FWM}}(\omega,\tau)$ as the *background spectrum*. It should be noted that an inclusion of interactions that provide for a decay on a long-time scale can be expected to have little effect on the short-time behavior. Since the background spectrum is almost exclusively determined by the decoherence on the short-time scale of a few tens of picoseconds it is safe to assume that the background spectrum will not change much by including long-time decay mechanisms in the model.

Similar to the time domain, a number of generic properties can be established for the frequency domain signals. Some of them follow directly from the time domain results discussed above. For example, from the fact that the envelope becomes real at large τ [cf. Eq. (18)] it can be concluded that the spectra obey the symmetry relation

$$\lim_{\tau\to\infty}G_{\mathrm{FWM}}(\omega,\tau)=\lim_{\tau\to\infty}G^*_{\mathrm{FWM}}(-\omega,\tau). \tag{29}$$

According to Eq. (27) this holds separately for the singular part G_s and is, therefore, also valid for the nonsingular part ΔG_{FWM} alone. Thus, the absolute value of the background spectrum evolves into a symmetric function of ω in the limit of long delay times. In contrast to this, the spectra at zero delay time exhibit an asymmetry which is especially pronounced at low temperatures. Physically this can be understood as follows: for $\tau\to 0$ the FWM signals coincide with the linear response as has been noted earlier. However, the imaginary part of the linear spectra [the real part of the Fourier transform of $G_{\mathrm{lin}}(t)$] is proportional to the light absorption, and the total energy of the absorbed light equals the energy of the created exciton plus or minus the energy of n phonons emitted or absorbed in the process. At $T=0$ there are no available phonons in the system and, consequently, only phonon emission can take place. Therefore, in the limit of vanishing temperature the linear spectra approach zero for frequencies below the resonance corresponding to the zero-phonon line. With rising temperature the corresponding spectra are in general still asymmetric, but the asymmetry is less pronounced.[33] Further insight can be obtained by expanding the background sprectrum $\Delta G_{\mathrm{FWM}}(\omega,\tau=0)$ at $T=0$ in a power series with respect to $|\gamma_q|^2$. This expansion can be derived most easily by expanding $\Delta G_{\mathrm{FWM}}(t,\tau=0)$ in a series and then taking the Fourier transform term by term. This results in

$$\lim_{T\to 0}\Delta G_{\mathrm{FWM}}(\omega,\tau=0)\propto\sum_q\frac{i|\gamma_q|^2\left(1-\sum_{q'}|\gamma_{q'}|^2\right)}{\omega-\omega_q+i\delta}+\sum_{q,q'}\frac{i|\gamma_q|^2|\gamma_{q'}|^2}{\omega-\omega_q-\omega_{q'}+i\delta}+\mathcal{O}(|\gamma|^6), \tag{30}$$

where the limit $\delta\to 0^+$ is implied. Using the identity

$$\lim_{\delta\to 0^+}\frac{1}{x-i\delta}=\mathcal{P}(1/x)+i\pi\delta(x), \tag{31}$$

where $\mathcal{P}$ denotes the principal value, it can be formally confirmed that, as expected, the real part of Eq. (30) vanishes identically for $\omega<0$. This property is indeed fulfilled separately for each term in the expansion [shown explicitly in Eq. (30) up to the second nonvanishing contribution]. Moreover, as $|\gamma_q|^2\propto 1/q$ for $q\to 0$ and because the volume element, obtained when the q sum is converted into an integral, scales as $\sim q^2$ it is seen that the real part of Eq. (30) goes to zero as ω approaches zero from the right. This is enough to conclude

that the spectrum of the FWM signal at small delays is a continuous function at $\omega=0$. It is therefore asymmetric and the maximum of its absolute value is shifted to a positive ω.

In the opposite limit $\tau\to\infty$, where the absolute value of the spectrum becomes a symmetric function, we expand Eq. (18) in a series and then take the Fourier transform. The first term of this expansion reads

$$\lim_{T\to 0}\Delta G_{\mathrm{FWM}}(\omega,\tau\to\infty)\propto\sum_q |\gamma_q|^2\left[\frac{i}{\omega-\omega_q+i\delta}+\frac{i}{\omega+\omega_q+i\delta}\right]+\mathcal{O}(|\gamma|^4). \tag{32}$$

This obviously yields for $\omega<0$ nonvanishing expressions even at $T=0$. Nevertheless, using the asymptotic properties of $|\gamma_q|^2$ for small q values and the relation Eq. (31) we can conclude in the same way as in the discussion of Eq. (30) that the real part of Eq. (32) vanishes in the limit $\omega\to 0$. Furthermore, irrespective of the form of $|\gamma_q|^2$, the imaginary parts on the right-hand side of Eq. (32) cancel when ω approaches zero. Therefore, when the first-order term in the expansion, Eq. (32), dominates, which should be true for not too large $|\gamma_q|^2$, it follows that the FWM spectrum at large delay times is symmetric and has a local minimum at $\omega=0$. Thus, only from basic asymptotic properties of $|\gamma_q|^2$ can it be deduced that the single dot FWM spectra at low temperatures are asymmetric for small delays, but with increasing delay time they transform into symmetric functions with a local minimum at $\omega=0$.

On the other hand, in the opposite limit of high temperatures the real-time FWM signal at zero delay time is, according to Eq. (22), represented by a Gaussian and therefore the corresponding spectrum is also a Gaussian; in particular it is a symmetric function with a single maximum at $\omega=0$. Analogous considerations for large τ values using Eq. (18) reveal that the corresponding spectra are symmetric also in this case.

Summarizing the results obtained so far we conclude that at high temperatures the spectra at different τ should be almost symmetric, have a single maximum near $\omega=0$, and be similar with respect to their line shapes. Indeed, one can trace this generic behavior in our numerical results presented below [cf. Fig. 3(b) below].

C. Form factor and optical signals

The aim here is to relate basic properties of the form factor for the carrier-phonon coupling to corresponding features of the optical signals. First, we note that the temporal behavior of the absolute values of the envelope functions for single dot FWM signals [cf. Eq. (6)], for the linear response [cf. Eq. (13)] as well as for the time-integrated FWM signal of an infinitly strong inhomogeneously broadened dot ensemble [cf. Eq. (15)], is given by exponentials which all contain a summation (integration) in the exponent. The integrand is in all cases a product of an oscillating factor, e.g., $1-\cos(\omega_q t)$ for the linear response in Eq. (13), and the time-independent factor

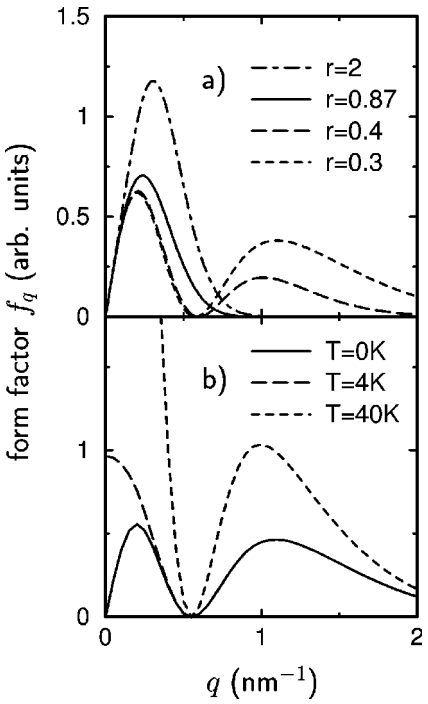

FIG. 1. Form factor for the carrier-phonon coupling f_q, (a) for different values of the ratio $r=a_h/a_e$ at $T=1$ K, and (b) for $r=0.3$ at the temperatures $T=0$ K, 4 K, and 40 K.

$$F_q=|\gamma_q|^2(1+2N_q). \tag{33}$$

Thus, the temporal behavior of the above three signals is governed by the same quantity F_q. However, since only integrated properties of F_q enter it should be expected that the signals are not sensitive to every detail of the line shape of F_q. Instead, many qualitative features should be related to only a few basic properties of F_q. In order to analyze this relation in more detail we concentrate on isotropic models where F_q and ω_q depend only on the modulus of the wave vector q and the angle integrations can be easily performed. The integrand of the remaining q integration is then given by

$$f_q:=\Gamma_q(1+2N_q)$$

with

$$\Gamma_q:=q^2|\gamma_q|^2. \tag{34}$$

We will refer to f_q as the form factor for the carrier-phonon coupling or if there is no risk of ambiguity simply speak of the form factor. It is the product of a temperature-independent factor Γ_q and the factor $1+2N_q$ which depends on T via the Bose distribution N_q.

In order to get a feeling for the typical structure of the form factor we have plotted f_q for our model in Fig. 1(a) for $T=1$ K for different values of the ratio $r:=a_h/a_e$ between the localization length a_h of the hole and a_e of the electron. At low temperatures the form factor is dominated by the temperature-independent factor Γ_q which according to our

model scales as $\Gamma_q \propto q$ in the limit $q \to 0$. In the opposite limit, $q \to \infty$, we find that $\Gamma_q \propto \exp(-q^2a^2/4)$, where $a = \min(a_e, a_h)$. Consequently, at least one maximum of Γ_q at a finite q value is ensured. For localization ratios $r > 1$ there is typically only a single maximum, as seen, e.g., in Fig. 1(a) for the $r = 2$ curve. When the hole is more strongly localized than the electron, i.e., $r < 1$, a second maximum appears, which grows in amplitude for smaller r. It is clearly visible in Fig. 1(a) for $r = 0.4$ and $r = 0.3$. In the case $r = 0.87$ it is also present but appears at a much larger q value and its amplitude is strongly suppressed. The appearance of the second maximum is a consequence of the cancellation of contributions from the electron and the hole to the phonon coupling γ_q in Eq. (7). These cancellations occur only for $r < 1$ because we have used parameters where the relation $|D_h| < |D_e|$ holds. Furthermore, it is required that D_h and D_e have equal signs. Then, indeed, one can see directly from Eqs. (2) and (3) that γ_q defined in Eq. (7) vanishes when

$$q = \frac{2}{a_e}\sqrt{\frac{\ln(|D_e/D_h|)}{1-r^2}}, \tag{35}$$

which is real only for $r < 1$ (since $|D_h| < |D_e|$).

Thus, the typical behavior of the factor Γ_q can be characterized as follows: Γ_q vanishes in the limits $q \to 0$ and $q \to \infty$ and has maxima (peaks) at finite q values; for a single dot characterized by ground-state wave functions, i.e., wave functions without any nodes, the number of maxima is typically either one or two. Already by considering only these basic properties we can deduce some qualitative features of the optical response. Let us explore the consequences of the fact that Γ is peaked at finite q values. In a first step we discuss the effect of a single peak at $q = Q$ which is infinitely sharp, i.e., we discuss a model for Γ_q defined by

$$\Gamma_q = \Gamma_Q \delta(q - Q) + \tilde{\Gamma}_q, \tag{36}$$

where $\tilde{\Gamma}_q$ is assumed to provide a structureless ''background'' in the vicinity of the peak at $q = Q$. The contribution of the peak to the integrals in Eqs. (6), (13), and (15) can be immediately evaluated in all three cases. For simplicity we will discuss explicitly the results for the linear response, Eq. (13). The nonlinear signals in Eqs. (6) and (15) can be analyzed along the same lines. Using Eq. (36) in Eq. (13) we obtain

$$|G_{\rm lin}(t)| = |\tilde{G}_{\rm lin}(t)| \exp\{-\Gamma_Q[1 - \cos(\omega_Q \tau)]\}, \tag{37}$$

where $|\tilde{G}_{\rm lin}(t)|$ denotes the contribution from the background which is evaluated from $\tilde{\Gamma}_q$. This background component is modulated by oscillations with the frequency ω_Q. It is important that although Γ_Q can be relatively small compared with the weight of the background part $\tilde{\Gamma}_q$, the corresponding modulation can still be noticeable. If two or more sharp peaks are present, the resulting modulation is a sum of the individual modulations, each oscillating with the corresponding frequency. Thus, we expect oscillations of the optical signals with a frequency given by ω_Q whenever Γ_q exhibits a sharp structure at $q = Q$. The phonon couplings $g_q^{e(h)}$ defined in Eq. (2), from which γ_q and therefore also Γ_q are derived, depend on both electronic properties [via the electronic form factor $\Psi^{e(h)}(\mathbf{q})$] and phononic properties. It is, therefore, clear that, in principle, structures in either of these can lead to corresponding sharp peaks in Γ_q. For example, if there is an enhanced density of phonon states in modes confined in the dot region then it is likely that the corresponding Γ_q exhibits a sharp structure at a q value $Q_{\rm dot}$ of the order of the reciprocal dot dimension and consequently corresponding optical signals should be modulated with the frequency $\omega_{Q_{\rm dot}}$. However, for the bulk modes that we use for the numerical evaluations in the present paper, the peaks have a finite width. The essential features of optical signals resulting from dots which, similar to our present model, exhibit peaks in Γ_q of a finite width can be captured in a simple Gaussian model

$$\Gamma_q = \frac{\Gamma_Q}{\sqrt{2\pi}\sigma}\exp\left[-\frac{(q-Q)^2}{2\sigma^2}\right] + \tilde{\Gamma}_q, \tag{38}$$

which represents a broadened peak on a smooth background $\tilde{\Gamma}_q$. Again we concentrate on the linear response given by Eq. (13). The analogous analysis of the FWM signals leads to similar conclusions. Assuming a linear phonon dispersion, $\omega_q = cq$, Eq. (13) separates for the model in Eq. (38) as follows:

$$G_{\rm lin}(t) = \tilde{G}_{\rm lin}(t) \exp[-\Gamma_Q e^{-(t^2c^2\sigma^2/2) - iQct}]. \tag{39}$$

As in the case of the delta peak the background part $\tilde{G}_{\rm lin}(t)$ is modulated by an oscillation, which in this case, however, decays with time. The oscillation has a period of $T_0 = 2\pi/(Qc)$ and the decay time is given by $t_0 \approx 1/(\sigma c)$. The number of oscillation periods that can be observed in such a system can, therefore, be estimated as $N \approx Q/\sigma$, i.e., by the ratio of the peak position and the corresponding peak width.

Looking at the peak structures in Fig. 1(a) we conclude that most of the peaks have a width comparable to their peak position. We therefore expect that in these cases the optical response should in general depend on the real time and the delay time in a nonmonotonous way, resembling an overdamped oscillation with only one resolved period. For example, for the $r = 0.87$ curve in Fig. 1(a) the dominant peak is located at about $Q = 0.3\ \mathrm{nm}^{-1}$ with about the same width corresponding to a modulation period of $T_0 \approx 4$ ps and a decay time of the same order of magnitude. Interestingly, some of the peaks occur at a Q position larger than their widths. For example, the curve for $r = 0.3$ has a peak at $Q \approx 1.1\ \mathrm{nm}^{-1}$, corresponding to an oscillation period of ≈ 1.1 ps with a noticeably smaller width. Here, we should expect more pronounced modulations of the corresponding signals. We will come back to this point later.

While the form factor f_q at zero temperature coincides with Γ_q, at finite temperatures it is also affected by the Boltzmann factor in Eq. (34). In Fig. 1(b) we have plotted f_q for three different temperatures and a fixed localization ration of $r = 0.3$. As can be seen from the figure, increasing the temperature leads to systematic changes with respect to the peak structures. Most notable, the form factor reaches a finite lim-

iting value when q approaches zero. This is due to the $1/q$ singularity of the Bose factor which cancels the $\sim q$ behavior of Γ_q. Expanding the Bose factor it is seen that the corresponding limiting value is proportional to the temperature. As a result of the Bose singularity, the first maximum moves towards $q=0$ and the amplitude of the first peak is strongly enhanced. Also the position of the second peak shifts towards lower q values. Within our simplified Gaussian model it is easy to prove explicitly that the peak positions should always shift towards lower q values with increasing temperatures. Indeed, for the temperature-dependent maximum $Q(T)$ of the product of the Gaussian in Eq. (38) and the temperature-dependent factor $1+2N_q$, we find

$$Q(T)=Q-2\sigma^2\hbar c\frac{N_{Q(T)}}{k_BT}\frac{1+N_{Q(T)}}{1+2N_{Q(T)}}. \tag{40}$$

This proves that the correction to the zero-temperature value Q is always negative and thus the period of the corresponding modulations increases with the temperature.

As suggested by the asymptotic Eq. (22), at large temperatures there should not be any phonon-induced oscillations present in the envelope functions discussed so far. In this limit the first peak completely dominates the form factor f_q. However, this peak moves to $q=0$ with increasing width. Consequently, the oscillation corresponding to this peak is increasingly damped and has a period which approaches infinity in accordance with our previous finding.

V. NUMERICAL RESULTS

The following subsections are meant to give a more quantitative impression of the signals predicted by our theory. In particular, we will present numerical results that have been obtained by applying the spherical model defined in Sec. II. We use standard GaAs parameters. The values of all material parameters used apart from the confinement lengths a_e and a_h are listed in Table I of Ref. 33.

A. Single dot FWM response

We start the discussion by analyzing FWM signals from a single quantum dot in the time domain. By using Eq. (6) we have plotted in Fig. 2 real-time traces of the FWM envelope $G_{\mathrm{FWM}}(t,\tau)$ for four different values of the delay time τ between the external light pulses. Figures 2(a) and 2(b) show the absolute value of the signals while the corresponding imaginary parts are shown in Figs. 2(c) and 2(d). Figures 2(a) and 2(c) are calculated for a temperature of $T=1$ K while for Figs. 2(b) and 2(d) a value of $T=30$ K has been used. We note that at $\tau=0$ the FWM response coincides with the linear response, Eq. (13) according to $G_{\mathrm{FWM}}(t,\tau=0)=G_{\mathrm{lin}}(t)$. Consequently, Fig. 2 also provides a comparison between FWM signals and the linear response (solid line in Fig. 2).

As expected from our previous analysis the absolute values are nonmonotonous functions that resemble overdamped oscillations. Also obvious from the figure is the general trend that the nonmonotonous modulations are more pronounced for lower temperatures. As usual for a two-pulse FWM signal the maximum value decreases with increasing delay. All curves exhibit a fast initial decay from their maximal values on a time scale of approximately $t_0\approx 1-2$ ps. As discussed earlier, after the initial drop all curves approach a nonzero value in the limit $t\to\infty$. In accordance with Eq. (16) we find that the long-time limiting value declines with increasing temperature and with increasing τ. A more quantitative analysis of the initial decay and the behavior of the limiting value is given below.

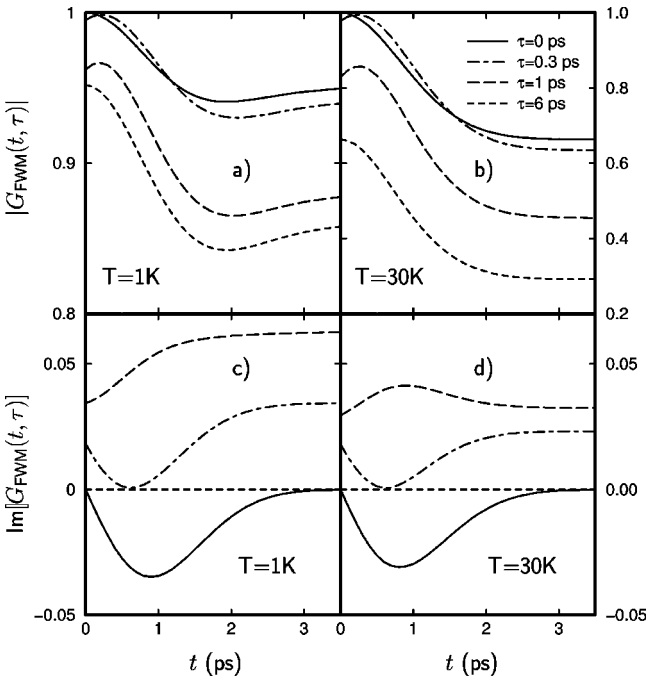

FIG. 2. Absolute value [(a) and (b)] and imaginary part [(c) and (d)] of the single dot FWM envelope function, $G_{\mathrm{FWM}}(t,\tau)$, calculated for $r=0.87$ and for different delays: $\tau=0$ ps (solid line), $\tau=0.3$ ps (dot-dashed line), $\tau=1$ ps (long-dashed line), $\tau=6$ ps (short-dashed line). (a) and (c) correspond to $T=1$ K and (b) and (d) to $T=30$ K. At $\tau=0$ the FWM signal envelope coincides with the envelope of the linear response.

By plotting the imaginary parts in Figs. 2(c) and 2(d) one can monitor the prediction that the envelope function $G_{\mathrm{FWM}}(t,\tau)$ should become real for long delay times [cf. Eq. (18)] which implies that the imaginary parts should vanish in this limit. As seen from Figs. 2(c) and 2(d) the expected limit is indeed reached after about 2 ps, but it is approached in a nonmonotonous way. For $\tau=0$ the imaginary part turns out to be entirely negative while for delays longer than 0.3 ps it is entirely positive. Furthermore, the shape also changes significantly with delay time. The most important feature, however, is that the imaginary part approaches zero after roughly the same time it takes the real-time signal to approach its finite limiting value. The reason for this result is revealed by looking at Eq. (6) which indicates that the properties of the FWM signals in the t and τ domains are qualitatively similar. One consequence of this symmetry has already been explicitly expressed in Eq. (18) where the corresponding long-time limits have been related to each other. The characteristic time at which the envelope changes as a function of both t and τ has been estimated in Ref. 48 to be approximately given by

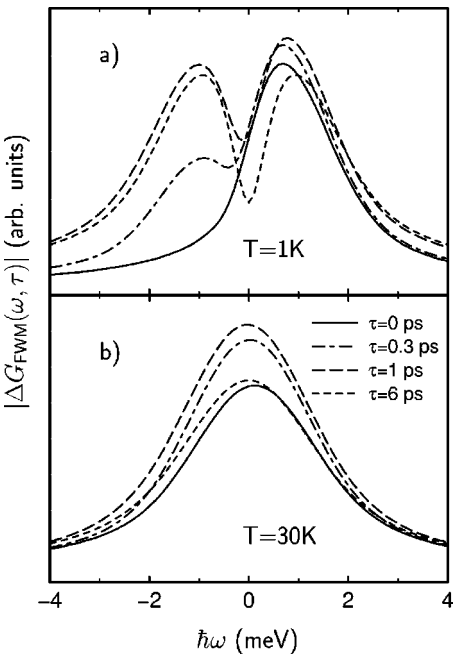

FIG. 3. Absolute value of the background spectra $\Delta G_{\mathrm{FWM}}(\omega,\tau)$ of the single dot FWM signal calculated according to Eq. (25) for $r=0.87$ and different delay times τ: (a) $T=1$ K and (b) $T=30$ K.

the time $t_{ph}=a/c$ needed for the phonons created in the excitation process to leave the dot (cf. also the Appendix). For $a\approx 4$ nm used in the current calculations this estimate gives $\tau\approx 1$ ps, which is of the right order of magnitude. Interestingly, only for delay times either much shorter or longer than this characteristic time the curves in Figs. 2(a) and 2(b) have their maximum at $t=0$, i.e., at the arrival of the second pulse. For intermediate delays the maximum is shifted towards finite real-time values.

The absolute value of the background spectra $\Delta G_{\mathrm{FWM}}(\omega,\tau)$ corresponding to the real-time FWM signals in Fig. 2 are plotted in Fig. 3(a) for $T=1$ K and in Fig. 3(b) for $T=30$ K. Clearly it is seen that the signals at low temperatures evolve from an asymmetric shape at $\tau=0$ (this curve coincides with the linear background spectrum) to a symmetric function for long delay times as discussed analytically in Sec. IV B. Indeed, at $\tau=6$ ps the absence of the imaginary part yields a symmetrical spectrum. Furthermore, in accordance with the conclusions drawn from the expansion in Eq. (32) the spectra exhibit a local minimum at $\omega=0$ for longer delay times. Also in agreement with our general considerations in Sec. IV B the spectra at higher temperatures are almost symmetric with a maximum near $\omega=0$ for all delay times. Interestingly, the absolute heights of the spectra change in a nonmonotonous way. Starting from $\tau=0$ the total spectral weight of the background spectra first increases for larger delays and then decreases again.

So far we have discussed a number of qualitative features that nicely illustrate our general results derived in the previous sections. From the figures some additional overall trends have become apparent which deserve to be analyzed on a more quantitative level. To this end we study the behavior of three quantities which quantify specific characteristics of the curves. The first quantity that is analyzed is the weight W_s of the singular part of the spectrum. According to Eq. (28) it is given by the amplitude $|G_{\mathrm{FWM}}|$ of the FWM envelope evaluated in the long-time limit $t\to\infty$. As discussed in Sec. IV B, W_s is also related to the spectral weight of the zero-phonon line. It is interesting to contrast the behavior of the singular part of the spectrum with the corresponding dependencies of the nonsingular contributions, i.e., of the background spectrum ΔG_{FWM}. In order to measure the total spectral weight of the background spectrum we introduce the quantity W_b defined as

$$W_b(\tau)^2=\int_{-\infty}^{\infty}|\Delta G_{\mathrm{FWM}}(\omega,\tau)|^2\frac{d\omega}{2\pi}=\int_0^{\infty}|\Delta G_{\mathrm{FWM}}(t,\tau)|^2dt. \tag{41}$$

Besides the analysis of the weights of singular and nonsingular parts of the spectrum it is also of interest to quantify the initial decay time. However, the temporal behavior of our signals is in general neither Gaussian nor exponential and also, in some cases (cf. Fig. 2), the maximum does not coincide with the onset of the signal set by the arrival of the second pulse. Therefore, there is not a distinguished measure for the initial decay, and several different choices are possible. We have chosen to identify the initial decay time with the time τ_0 it takes from the arrival of the second pulse to reach the point at which the signal has dropped half way from its initial value towards the corresponding long-time limit. Looking at the line shapes of our signals it is seen that the above prescription uniquely defines a measure for the duration of the initial decay.

The delay-time dependence of the three quantities W_s, W_b, and τ_0 has been calculated for the temperatures $T=1$, 30, and 100 K and the results are displayed in Fig. 4. First, we note that the limiting value $W_s=|G_{\mathrm{FWM}}(\infty,\tau)|$ is typically a decreasing function of τ similar to the real-time dependence in Figs. 2(a) and 2(b). This reflects once again the approximate symmetry between the real- and delay-time regimes. A close look at Fig. 4(a) reveals a slightly nonmonotonous decay at $T=1$ K, while at the larger temperatures the curves drop monotonously towards their limiting values. As expected from the formulas in Eqs. (16) and (17) we find that W_s drops significantly with increasing temperature. Figure 4(b) quantifies what we have noted earlier that the weight of the background spectrum is a nonmonotonous function of the delay time. Typically, a single maximum is found at a finite delay time. With increasing temperature the maximum is more pronounced and its value is shifted towards earlier times. The crossing of the $T=30$ K and the $T=100$ K curves indicates that W_b also depends in a nonmonotonous way on the temperature.

Interestingly, the delay-time dependence of the initial decay time τ_0 shown in Fig. 4(c) changes its character with rising temperature: at $T=1$ K it decreases monotonously, while for higher temperatures it evolves into a nonmonotonous function of the delay time. In particular, τ_0 has a maximum at a finite delay time. This means that at intermediate temperatures it should be possible to optimize the decay of

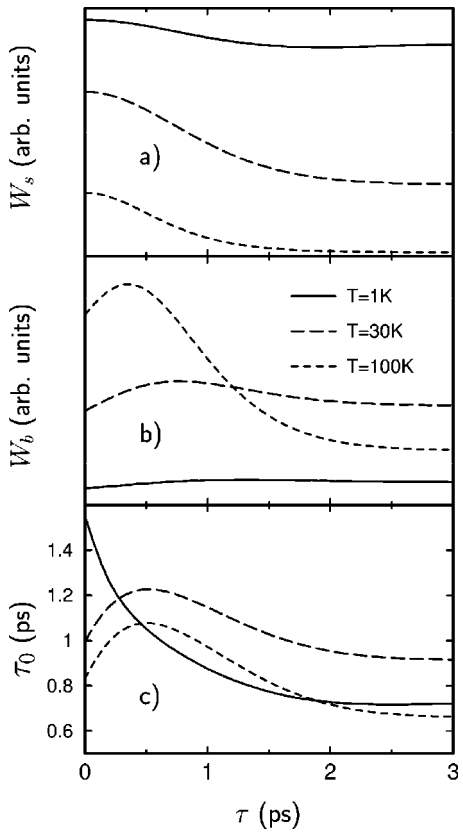

FIG. 4. (a) Spectral weight W_s of the singular part of the spectrum. W_s coincides with the amplitude of the long-time limiting value of the signal. (b) Spectral weight W_b of the background spectrum defined by Eq. (41). (c) Initial decay time τ_0. All quantities are plotted as functions of the delay time τ for $r=0.87$ and for three different temperatures: $T=1$ K (solid line), $T=30$ K (long-dashed line), and $T=100$ K (short-dashed line).

the optical response towards longer decoherence times by suitably tuning the delay time. Figure 4(c) also indicates that the initial decay time is not necessarily a decreasing function with rising temperature.

B. FWM signals from dot ensembles

A widespread application of FWM experiments is to measure the homogeneous linewidth in strongly inhomogeneously broadened systems. Linear absorption measurements on such systems reflect almost exclusively the width of the inhomogeneous broadening and give no clue to the intrinsic homogeneous decay time. Often the previously mentioned relation between the time-integrated FWM signal from an infinitely broadened system and the square of the linear response from a homogeneously broadened sample is taken as the basis for this extraction. However, by comparing Eq. (15) with Eq. (13) it was noted before that the expressions for the envelope $\overline{G_\infty}$ of an infinitely inhomogeneous broadened ensemble and for the single dot linear envelope function $|G_{\rm lin}|^2$ are similar but do not coincide. Thus, in contrast to a dephasing model with phenomenological damping rates the above relation is not strictly fulfilled within our model. Figures 5(a) and 5(c) provide a direct comparison of these functions. In

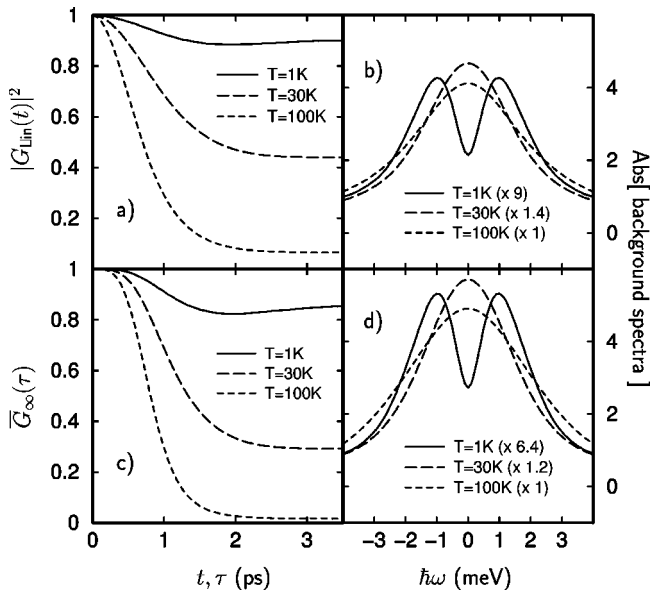

FIG. 5. (a) Absolute square $|G_{\rm lin}|^2$ of the linear response as a function of the real time t. (b) Absolute value of the background spectra corresponding to (a). (c) Normalized time-integrated FWM amplitudes $\overline{G_\infty}$ from an ensemble with infinitely strong inhomogeneous broadening as a function of the delay time τ. (d) Absolute value of the background spectra corresponding to (c). All quantities are plotted for $r=0.87$ and for three temperatures: $T=1$ K (solid line), $T=30$ K (long-dashed line), and $T=100$ K (short-dashed line).

Fig. 5(a) we have plotted $|G_{\rm lin}|^2$ as a function of real time for three different temperatures while Fig. 5(b) displays $\overline{G_\infty}$ as a function of the delay time for the same temperatures. Obviously, the corresponding temporal line shapes are very similar. Qualitatively, the behavior is also similar to the single dot real-time traces for short or long delay times shown in Figs. 2(a) and 2(b). For temperatures above ~ 10 K the curves decay monotonously towards a finite limiting value while at low temperatures ~ 1 K a strongly overdamped oscillation is observed which provides for a slight modulation of the decay. In agreement with the asymptotic formulas, Eq. (21) and Eq. (19), we find that the initial drop is significantly deeper for the FWM signal than for $|G_{\rm lin}|^2$. However, the time scale for the drop turns out to be roughly the same.

Following the procedure of Sec. IV B, it is possible to define background spectra corresponding to the functions $\overline{G_\infty}$ and $|G_{\rm lin}|^2$. Of course, the Fourier transform has to be performed with respect to the delay time in the former case and with respect to the real time in the latter case. The absolute values of these spectra are displayed in Fig. 5(b) for $|G_{\rm lin}|^2$ and in Fig. 5(d) for $\overline{G_\infty}$. Since the time domain functions are real in both cases the corresponding Fourier transforms obey the symmetry relation $f(\omega)=f^*(-\omega)$ and consequently the real parts of the spectra are symmetric functions of ω. Comparing the FWM spectra with their counterparts calculated for $|G_{\rm lin}|^2$ it is seen that in both cases very similar line shapes are obtained with only minor differences concerning the corresponding widths. As in the low temperature single dot spectra in Fig. 3, in Figs. 5(b) and 5(d) a local minimum

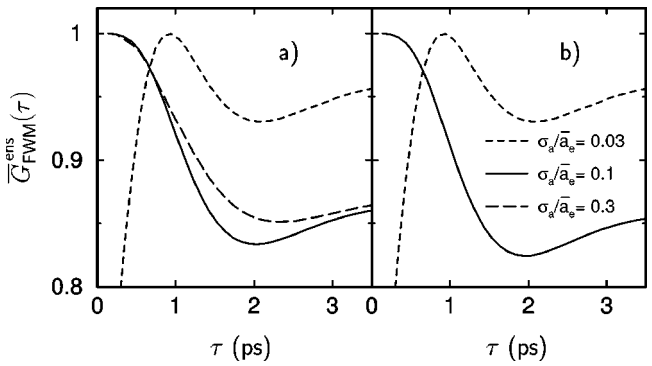

FIG. 6. Time-integrated FWM response $\overline{G}^{\mathrm{ens}}_{\mathrm{FWM}}$ as a function of the delay τ at $T=0.1$ K for different relative widths $\sigma_a/\overline{a_e}$ of the dot size distribution and fixed $r=\overline{a_h}/\overline{a_e}=0.87$. (a) Accounts for variations of the energies and carrier-phonon couplings caused by the size fluctuations, while (b) only accounts for energy fluctuations. The curves are normalized according to Eq. (11) except for the $\sigma_a/\overline{a_e}=0.03$ curve which is normalized to its maximum.

appears at $\omega=0$ due to the same reason: the suppression of the phonon coupling in the limit $q\rightarrow 0$. For the infinitely broadened ensemble this dip has already been reported in Ref. 48. For higher temperatures the dip disappears. Despite the good agreement with respect to the line shapes it is clearly seen that the absolute spectral weights of corresponding curves in Figs. 5(b) and 5(d) differ noticeably (note the scaling). In conclusion, we have found that apart from substantial differences with respect to the depths of the initial drop and the weights of the background spectra it is a rather good approximation to identify $\overline{G}_\infty$ with $|G_{\mathrm{lin}}|^2$. Especially in view of the fact that the shapes of the single dot spectra may change significantly with the delay time (cf. Fig. 3) this good agreement is quite remarkable.

We will now analyze the way in which the results are affected by the strength of the inhomogeneous broadening. Figure 6(a) shows ensemble-averaged time-integrated FWM signals calculated from Eqs. (9) and (11) for different values of the relative standard deviation $\sigma_a/\overline{a_e}$. These calculations have been performed for a rather low temperature of $T=0.1$ K in order to show most clearly the effect of inhomogeneous broadening on the nonmonotonous modulations which are more pronounced at low temperatures. For the low value of $\sigma_a/\overline{a_e}=0.03$ the signal is almost unbroadened and the echo has a rather large real-time extent. Consequently, for delay times shorter than the width of the echo the time-integrated signals are strongly suppressed because the echo is not yet fully developed. The result is a pronounced maximum at a finite delay time which is located at a time roughly corresponding to the temporal extent of the fully developed echo. To facilitate the comparison we have normalized this curve to its maximum rather than using Eq. (11). Starting from their maxima all curves exhibit a modulated decay. Surprisingly, the percentage drop from the maximum to the limiting value at large delay times depends nonmonotonously on the strength of the size fluctuations. Increasing $\sigma_a/\overline{a_e}$ from 0.03 to 0.1 leads to a significant enhancement of the percentage decrease while a further rise of $\sigma_a/\overline{a_e}$ to 0.3 reduces the drop. Interestingly, also the initial decay time gets noticeably longer when the fluctuations change from $\sigma_a/\overline{a_e}=0.1$ to $\sigma_a/\overline{a_e}=0.3$. The latter effect seems to be related to the fact that for fluctuations larger than $\sigma_a/\overline{a_e}=0.1$ the modulation flattens with increasing $\sigma_a/\overline{a_e}$.

As already noted, fluctuations of the dot sizes lead to variations of both the carrier energies and the carrier-phonon coupling. In order to get more insight into their respective roles we have performed calculations where only the effect of the energy fluctuations is kept, i.e., in these calculations the carrier-phonon coupling has been determined by using a fixed dot size corresponding to the mean value $\overline{a_e}$. The results are plotted in Fig. 6(b) for the same values of $\sigma_a/\overline{a_e}$ as in Fig. 6(a). It turns out that the curves calculated only accounting for energy fluctuations are almost indistinguishable for $\sigma_a/\overline{a_e}=0.03$ and 0.1 from their counterparts in Fig. 6(a) where changes of the carrier-phonon couplings have also been taken into account. Thus, for size fluctuations up to about 10% the effects related to the corresponding energy fluctuations clearly dominate. In this case changes of the envelope function G_{FWM} can be disregarded in Eq. (9). Here, the variations of the depth of the drop are, therefore, caused only by the corresponding changes of the temporal width of the echo. A temporally broader echo implies that the time-integrated signals effectively sample over a larger time window thus averaging out large temporal variations of the signal amplitudes. This is the main reason for the increase of the percentage drop when the fluctuation is increased from $\sigma_a/\overline{a_e}=0.03$ to $\sigma_a/\overline{a_e}=0.1$. However, when the energy distribution gets broader than the width of a typical single dot response, the echo is already sharp on the time scale on which the envelope G_{FWM} changes. A further increase of the broadening has therefore no effect on the signal. This is clearly seen in Fig. 6(b) in which the curves for $\sigma_a/\overline{a_e}=0.1$ and $\sigma_a/\overline{a_e}=0.3$ are indistinguishable. In contrast, the corresponding curves in Fig. 6(a) are substantially different, indicating that for size fluctuations above 10% the corresponding variations of the carrier-phonon couplings become indeed important and can no longer be ignored. These results imply that the discussion in the previous sections based on the function $\overline{G}_\infty$, where infinitely strong energy fluctuations have been assumed together with fixed values of the carrier-phonon coupling, is indeed representative for a system with an energy distribution broader than the width of a single dot spectrum but with size variations not much larger than 10%.

In Sec. V A we have characterized the behavior of single dot FWM signals by three quantities: the weights W_s and W_b of singular and background parts of the spectrum and the time τ_0 measuring the initial decay time. Obviously, analogous quantities can be introduced for the time-integrated and ensemble-averaged signals $\overline{G}^{\mathrm{ens}}_{\mathrm{FWM}}(\tau)$ as well as for the absolute square of the linear response $|G_{\mathrm{lin}}(t)|^2$. Here, there is only one time argument, namely, the delay time in the former case and the real time in the latter case, and the Fourier transformation defining the spectra has to be taken with re-

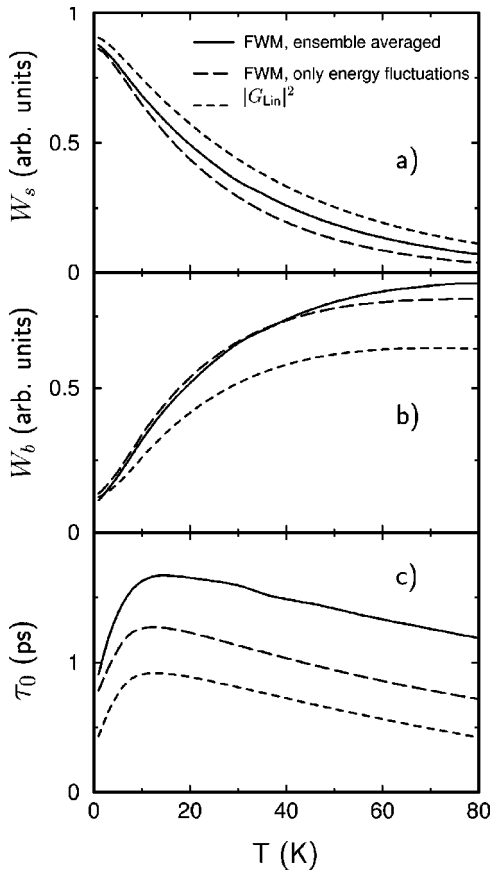

FIG. 7. (a) Spectral weight W_s of the singular part of the spectrum. W_s coincides with the amplitude of the long-time limiting value of the signal. (b) Spectral weight W_b of the background spectrum. (c) Initial decay time τ_0. All quantities are plotted as functions of the temperature for $r=\overline{a_h}/\overline{a_e}=0.87$: (solid line) $\overline{G}^{\rm ens}_{\rm FWM}$, calculated with $\sigma_a/\overline{a_e}=0.3$; (long-dashed line) $\overline{G}^{\rm ens}_{\rm FWM}$, calculated with $\sigma_a/\overline{a_e}=0.3$ neglecting the variations of the carrier-phonon couplings, and (short-dashed line) $|G_{\rm lin}|^2$.

spect to this argument. In Fig. 7 these quantities are plotted as functions of the temperature T. In addition, Fig. 7 also displays a curve calculated for the ensemble-averaged response $\overline{G}^{\rm ens}_{\rm FWM}(\tau)$ where only fluctuations of the energies have been accounted for. The calculations have been performed for a relative standard deviation of $\sigma_a/\overline{a_e}=0.3$. For this value of $\sigma_a/\overline{a_e}$ the results obtained without accounting for variations of the carrier-phonon-coupling have already reached the limit of infinite broadening described by $\overline{G}_\infty$ as can be seen from Fig. 6.

According to Fig. 7(a) the weight of the singular part W_s, which is also the long-time limiting value of the response, monotonously decreases with temperature in agreement with Eq. (22). All three curves are rather close. They confirm the general trend that the absolute square of the linear response yields a W_s which is systematically higher than the FWM results. Also the drop of the long-time limiting value found in Fig. 6, when the fluctuations of the carrier-phonon coupling are switched off, turns out to be a systematic feature observed for all temperatures.

In contrast to W_s the weight of the background spectrum W_b in Fig. 7(b) differs considerably for the linear and FWM signals. This was already noted in Fig. 5. In addition, the effect of fluctuations of the carrier-phonon coupling on W_b reverses with temperatures: above $T\approx 40$ K the weight of the background spectrum is enhanced by these fluctuations while at lower temperatures it is slightly suppressed.

Contrary to what might be expected intuitively, the initial decay time [Fig. 7(c)] is a nonmonotonous function of the temperature. The decay time decreases for high temperatures with a rate that can be extracted from the asymptotic expansion, Eq. (22), to be

$$\tau_0 \approx \sqrt{\frac{\hbar}{kTc^2\Gamma}}. \tag{42}$$

However, it increases with T for temperatures below 15 K for both the linear response and the FWM response irrespective of whether fluctuations of the carrier-phonon coupling are accounted for. This rather surprising finding can be understood as follows: In Sec. IV C it was concluded that the temporal behavior of the optical envelope functions consists in general of one or more damped oscillations depending on the peak structure of the form factor. The oscillation period is determined by the corresponding peak position while the damping is related to the width of the peak. With rising temperature the peak at the lowest q value has a rapidly growing amplitude and eventually dominates. Its position moves towards $q=0$ while its width increases. In addition it was shown that the position of the second peak is always shifted towards smaller q values (cf. Fig. 1). The increase of the width of the first peak alone would always lead to a stronger damping and therefore to a shorter initial decay time. However, the shift of the peak positions towards lower q values implies longer oscillation periods and thus the first minima of the oscillations are moved towards later times. But moving the first minimum to a later time in the case of an overdamped oscillation implies that the curve decreases on a longer-time scale, i.e., a longer decay time is observed. Obviously, this mechanism is effective only at low temperatures. At higher temperatures the first peak has reached the vicinity of $q\approx 0$ and dominates. Thus, oscillatory structures are effectively suppressed and the high-temperature limit described by Eq. (42) is approached. The interplay of these effects results in the nonmonotonous temperature dependence of τ_0 in Fig. 7(c).

It is also worth noting that in agreement with Fig. 6 the initial decay takes a noticeably longer time when both energy and carrier-phonon couplings fluctuate than in a system where only energy fluctuations take place. The shortest initial decay times are found for the absolute square of the linear response.

C. Phonon-induced modulation of the optical response

So far we have studied signals for a fixed localization ratio $r=0.87$. From Fig. 1(a) we learned that the form factor in this case is dominated by the maximum with the lowest possible q value. For $T=1$ K it is located at $Q\approx 0.3$ nm^{-1},

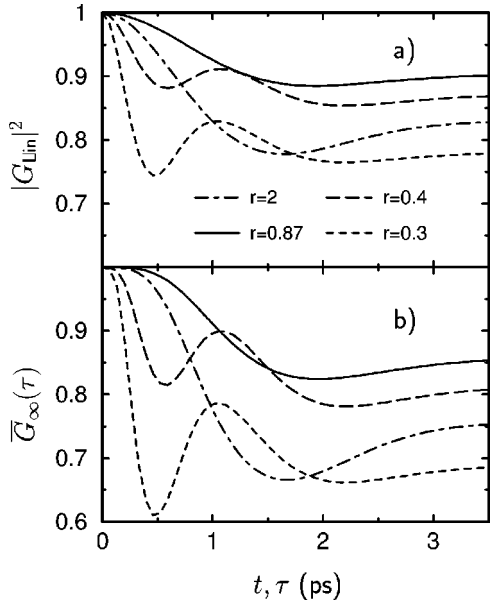

FIG. 8. (a) Absolute square of the linear response $|G_{\rm lin}|^2$ as a function of real time t. (b) Normalized time-integrated FWM amplitude $\overline{G}_\infty$ as a function delay time τ for different values of the localization ratio r: $r=2$ (dot dashed), $r=0.87$ (solid), $r=0.4$ (long dashed), and $r=0.3$ (short dashed).

with a full width that is of the same order of magnitude. The position of the first minimum of the oscillation is given by half the period, i.e., at $T_0/2\approx 2$ ps. This value is in good agreement with the position of the minimum in the $T=1$-K response in Figs. 2, 5, and 6. However, the oscillatory nature of the response is masked in this case because a completely overdamped situation has been realized. Already in Sec. IV C it was noted that for lower localization ratios a second maximum appears in the form factor which may not necessarily be in the fully overdamped limit. In order to investigate quantitatively the corresponding consequences we have plotted in Fig. 8(a) the linear response $|G_{\rm lin}|^2$ and in Fig. 8(b) the time-integrated FWM envelope $\overline{G}_\infty$ corresponding to an infinitely strong inhomogeneously broadened ensemble for different values of r at a temperature of $T=1$ K. For $r<0.6$ the second peak in the form factor is well separated from the first. The corresponding oscillations for the values $r=0.3$ and $r=0.4$ are clearly visible in Fig. 8 both in the linear response as well as in the FWM response. From the corresponding peak positions one deduces a half period of approximately 0.55 ps, in good agreement with the positions of the minima in Fig. 8. Thus, it is indeed the second peak in the form factor that governs the observed oscillations. The most remarkable point here, however, is the fact that clearly visible phonon-induced oscillations appear although the phonons form a smooth continuum without any structure in the dispersion ω_q or in the density of states. According to our analysis of the origin of the second peak in Sec. IV C they are due to the competition of electron and hole contributions to the carrier-phonon coupling.

VI. CONCLUDING REMARKS

In this work we have presented a comprehensive study of the impact of pure dephasing on FWM signals emitted from single quantum dots in the strong confinement regime and from corresponding dot ensembles. We have concentrated on effects induced by the coupling of the carriers trapped in the dot to LA phonons. By using exact closed-form formulas that are nonperturbative with respect to the carrier-phonon as well as the carrier-light-field coupling we were able to establish a number of generic features of the signals which do not depend critically on details of the carrier wave functions or the phonon couplings. These features were then quantified within a model of a spherical quantum dot coupled to isotropic bulk acoustic phonons. By using this model we explored the dependencies of FWM signals on the temperature, the delay time, as well as on the localization ratio r between holes and electrons. In particular, we concluded that the FWM signals from a single dot should coincide for zero delay time $\tau=0$ with the corresponding linear response. The maximum of the real-time response coincides with the arrival of the second pulse only for delay times that are either much shorter or much longer than typical phonon periods; for delay times of the order of the most efficiently coupled phonon modes the maximum is shifted towards later times. From their maximum value, the real-time single dot FWM signals drop at an initial rate which, at not too low temperatures, depends nonmonotonously on the delay time. Eventually, the signals reach a finite limiting value. At low temperatures the single dot FWM spectra evolve from an asymmetric form at $\tau=0$ into a symmetric function of ω for delay times larger than the initial decay time of the real-time response. The spectra at finite delays typically show a local minimum at the position of the zero-phonon line which is related to a reduced phonon coupling in the limit of small q values. A similar feature is found for the Fourier transform of time-integrated FWM signals emitted from dot ensembles. At elevated temperatures the limiting value of the signals decays exponentially with increasing temperature and all spectra are approximately symmetric. The corresponding line shapes do not change significantly with delay time and exhibit a maximum at the position of the zero-phonon line. The weights of the background spectrum W_b and the singular part of the spectrum W_s (the latter also includes the zero-phonon line) show very different dependencies on the temperature and the delay time. W_s is typically a decaying function of τ and T for a single quantum dot while W_b may exhibit a pronounced nonmonotonous dependence on these parameters.

The temporal and spectral line shapes of the time-integrated FWM signal from an infinitely inhomogeneously broadened dot ensemble are shown to be similar to the absolute square of the linear response of a single dot, a relation often used in order to extract information about the homogeneous broadening of the system from FWM experiments on dot ensembles. However, the depth of the initial drop as well as the spectral weight of the background spectrum are significantly different for these two signals.

The role of inhomogeneous broadening has been further investigated by considering time-integrated FWM signals from dot ensembles with varying strengths of dot size fluctuations. For size fluctuations up to about 10% the effect of the corresponding energy fluctuations is clearly dominant. For larger fluctuations of the sizes one has to take into ac-

count also the variations of the carrier-phonon coupling strengths. The latter result in longer initial decay times and in an enhanced long-time limiting value of the signal, when the strength of the size fluctuations is increased.

A rather unexpected result was the finding that the initial decay time is a nonmonotonous function of temperature. For temperatures below 15 K the signals initially decay on longer times for higher temperatures. This result has been explained by a shift of the peak in the form factor towards lower q values resulting in a shift of the first minimum of the corresponding overdamped oscillation towards later times.

Another interesting outcome of our analysis is the result that even for a bulk model of acoustic phonons with a linear energy dispersion $\omega_q = cq$, well-resolved oscillations of the corresponding optical response may be observed. These oscillations result from a second peak in the carrier-phonon form factor which occurs due to cancellations between electron and hole contributions to the coupling. For holes localized much more strongly than electrons this second peak is well separated from the first and the corresponding oscillations are clearly visible in the FWM as well as in the linear response, although the electronic wave functions are smooth and the phonons provide for a continuum of modes with no particular structures in the corresponding density of states.

ACKNOWLEDGMENTS

This work has been supported by the European Commission within the FET Project No. IST-1999-11311 (Semiconductor-based implementation of quantum information devices).

APPENDIX: DERIVATION OF ASYMTOTIC FORMULAS

The asymptotic formulas, Eqs. (16), (18), (19), and (21), for the behavior of the optical envelope functions in the long-time limit can all be derived according to the same scheme. Here, we will explicitly discuss the derivation of Eq. (19) for $\overline{G}_\infty(\tau \to \infty)$.

Our starting point is Eq. (15) which can be written as

$$\overline{G}_\infty(\tau) = \exp\{-2A(\tau)\}, \tag{A1}$$

where the function $A(\tau)$, after converting the q sum into an integral and performing the angle integrations, is given by

$$A(\tau) := \frac{2V}{(2\pi)^2}\int_0^\infty dq q^2 |\gamma_q|^2 (1+2N_q)[1-\cos(\omega_q \tau)]^2. \tag{A2}$$

Here, V is the normalization volume. First, we note that the integral in Eq. (A2) exists in the conventional sense, because it was assumed that $|\gamma_q|^2$, apart from the point $q=0$, is a smooth function which decays sufficiently fast for large q values. At the point $q=0$ we assume that the singular behavior is not stronger than $|\gamma_q|^2 \propto 1/q$. As discussed in Ref. 33 this is the strongest singularity that appears for the most commonly used carrier-phonon coupling schemes when the system is neutral overall. From this assumption it follows that the total integrand in Eq. (A2) has no singularity at $q=0$, because $N_q \propto 1/q$ and thus the singularities of $|\gamma_q|^2$ and N_q are canceled by the factor q^2 from the surface element. Using the identity $[1-\cos(\omega_q \tau)]^2 = 1 - 2\cos(\omega_q \tau) + 1/2[1 + \cos(2\omega_q \tau)]$ together with the linear dispersion $\omega_q = cq$ we find that $A(\tau)$ can be expressed in terms of the function

$$\mathcal{F}(x) := \frac{2V}{(2\pi)^2}\int_0^\infty dq f_q e^{iqx}, \tag{A3}$$

where the definition, Eq. (34), of the form factor f_q has been used. The function $A(\tau)$ can now be written as

$$A(\tau) = \frac{3}{2}\mathcal{F}(0) - \mathcal{F}(c\tau) - \mathcal{F}(-c\tau) + \frac{\mathcal{F}(2c\tau) + \mathcal{F}(-2c\tau)}{4}. \tag{A4}$$

However, apart from constant prefactors, $\mathcal{F}(x)$ is the Fourier transform of the function $\Theta(q) f_q$. Due to elementary properties of the Fourier transformation it thus vanishes for large arguments $|x| \to \infty$ as long as f_q does not exhibit singularities. Therefore, the limiting value of $A(\tau)$ for $\tau \to \infty$ can easily be read off from Eq. (A4) without further calculation.

This derivation also quantifies the relation between the decay properties of the Fourier transform of the form factor and the time scale on which the optical envelope functions approach their limiting values. The simple estimation given in the main text was based on the observation that f_q should be localized in q space roughly on a scale given by the inverse spatial extension of the dot due to the presence of the carrier form factor $\Psi^{e(h)}(\mathbf{q})$ in the carrier-phonon coupling [cf. Eqs. (2) and (3)]. This implies that $\mathcal{F}$ falls off on a length scale given by the dot extension a and therefore the typical time scale for the variation of the optical envelope functions is approximately given by the time $t_{ph} = a/c$ an emitted phonon needs to leave the dot.

[1] N. H. Bonadeo, J. Erland, D. Gammon, D. Park, D. S. Katzer, and D. G. Steel, Science **282**, 1473 (1998).

[2] N. H. Bonadeo, G. Chen, D. Gammon, D. S. Katzer, D. Park, and D. G. Steel, Phys. Rev. Lett. **81**, 2759 (1998).

[3] P. Borri, W. Langbein, S. Schneider, U. Woggon, R. L. Sellin, D. Ouyang, and D. Bimberg, Phys. Rev. Lett. **87**, 157401 (2001).

[4] T. H. Stievater, X. Li, D. G. Steel, D. Gammon, D. S. Katzer, and D. Park, Phys. Rev. B **65**, 205319 (2002).

[5] M. Betz, S. Trumm, A. Leitenstorfer, E. Behm, H. Krenner, M. Bichler, A. Zrenner, and G. Abstreiter, Phys. Status Solidi B **233**, 401 (2002).

[6] T. Guenther, C. Lienau, T. Elsaesser, M. Glanemann, V. M. Axt,

T. Kuhn, S. Eshlaghi, and A. D. Wieck, Phys. Rev. Lett. **89**, 057401 (2002).
[7] L. V. Dao, M. Lowe, P. Hannaford, H. Makino, T. Takai, and T. Yao, Appl. Phys. Lett. **81**, 1806 (2002).
[8] D. Loss and D. P. DiVincenzo, Phys. Rev. A **57**, 120 (1998).
[9] P. Zanardi and F. Rossi, Phys. Rev. Lett. **81**, 4752 (1998).
[10] A. Imamoglu, D. D. Awschalom, G. Burkard, D. P. DiVincenzo, D. Loss, M. Sherwin, and A. Small, Phys. Rev. Lett. **83**, 4204 (1999).
[11] M. S. Sherwin, A. Imamoglu, and T. Montroy, Phys. Rev. A **60**, 3508 (1999).
[12] G. Burkard, D. Loss, and D. P. DiVincenzo, Phys. Rev. B **59**, 2070 (1999).
[13] E. Biolatti, R. C. Iotti, P. Zanardi, and F. Rossi, Phys. Rev. Lett. **85**, 5647 (2000).
[14] F. Troiani, U. Hohenester, and E. Molinari, Phys. Rev. B **62**, R2263 (2000).
[15] T. Tanamoto, Phys. Rev. A **61**, 022305 (2000).
[16] P. Chen, C. Piermarocchi, and L. J. Sham, Phys. Rev. Lett. **87**, 067401 (2001).
[17] H. Kamada, H. Gotoh, J. Temmyo, T. Takagahara, and H. Ando, Phys. Rev. Lett. **87**, 246401 (2001).
[18] T. H. Stievater, X. Li, D. G. Steel, D. Gammon, D. S. Katzer, D. Park, C. Piermarocchi, and L. J. Sham, Phys. Rev. Lett. **87**, 133603 (2001).
[19] H. Htoon, T. Takagahara, D. Kulik, O. Baklenov, A. L. Holmes, and C. K. Shih, Phys. Rev. Lett. **88**, 087401 (2002).
[20] P. Borri, W. Langbein, S. Schneider, U. Woggon, R. L. Sellin, D. Ouyang, and D. Bimberg, Phys. Rev. B **66**, 081306(R) (2002).
[21] P. Borri, W. Langbein, S. Schneider, U. Woggon, R. L. Sellin, D. Ouyang, and D. Bimberg, Phys. Status Solidi B **233**, 391 (2002).
[22] A. Zrenner, E. Beham, S. Stufler, F. Findeis, M. Bichler, and G. Abstreiter, Nature (London) **418**, 612 (2002).
[23] F. Gindele, U. Woggon, W. Langbein, J. M. Hvam, K. Leonardi, D. Hommel, and H. Selke, Phys. Rev. B **60**, 8773 (1999).
[24] H. P. Wagner, H.-P. Tranitz, H. Preis, W. Langbein, K. Leosson, and J. M. Hvam, Phys. Rev. B **60**, 10 640 (1999).
[25] P. Borri, W. Langbein, J. Mørk, J. M. Hvam, F. Heinrichsdorff, M.-H. Mao, and D. Bimberg, Phys. Rev. B **60**, 7784 (1999).
[26] D. Birkedal, K. Leosson, and J. M. Hvam, Phys. Rev. Lett. **87**, 227401 (2001).
[27] Y. Masumoto, M. Ikezawa, B. R. Hyun, K. Takemoto, and M. Furuya, Phys. Status Solidi B **224**, 613 (2001).
[28] K. Takemoto, B. R. Hyun, and Y. Masumoto, Solid State Commun. **114**, 521 (2000).
[29] T. Takagahara, Phys. Rev. B **60**, 2638 (1999).
[30] L. Besombes, K. Kheng, L. Marsal, and H. Mariette, Phys. Rev. B **63**, 155307 (2001).
[31] P. Palinginis and H. Wang, Appl. Phys. Lett. **78**, 1541 (2001).
[32] S. V. Goupalov, R. A. Suris, P. Lavallard, and D. S. Citrin, Nanotechnology **12**, 518 (2001).
[33] B. Krummheuer, V. M. Axt, and T. Kuhn, Phys. Rev. B **65**, 195313 (2002).
[34] U. Bockelmann and G. Bastard, Phys. Rev. B **42**, 8947 (1990).
[35] H. Benisty, Phys. Rev. B **51**, 13 281 (1995).
[36] T. Takagahara, Phys. Rev. Lett. **71**, 3577 (1993).
[37] A. V. Uskov, A.-P. Jauho, B. Tromborg, J. Mørk, and R. Lang, Phys. Rev. Lett. **85**, 1516 (2000).
[38] S. Hameau, Y. Guldner, O. Verzelen, R. Ferreira, G. Bastard, J. Zeman, A. Lemaître, and J. M. Gérard, Phys. Rev. Lett. **83**, 4152 (1999).
[39] L. Jacak, J. Krasnyj, D. Jacak, and P. Machnikowski, Phys. Rev. B **65**, 113305 (2002).
[40] L. Jacak, J. Krasnyj, and W. Jacak, Phys. Lett. A **304**, 168 (2002).
[41] L. Jacak, P. Machnikowski, J. Krasnyj, and P. Zoller, Eur. Phys. J. D **22**, 319 (2003).
[42] O. Verzelen, R. Ferreira, and G. Bastard, Phys. Rev. Lett. **88**, 146803 (2001).
[43] O. Verzelen, G. Bastard, and R. Ferreira, Phys. Rev. B **66**, 081308(R) (2002).
[44] P. Lelong and S. H. Lin, Appl. Phys. Lett. **81**, 1002 (2002).
[45] V. M. Axt and S. Mukamel, in *Nonlinear Optical Materials*, edited by J. V. Maloney, Vol. 101 of *IMA Volumes in Mathematics and Its Applications* (Springer, Berlin, 1998), pp. 1–32.
[46] V. M. Axt, M. Herbst, and T. Kuhn, Superlattices Microstruct. **26**, 117 (1999).
[47] D. Steinbach, G. Kocherscheidt, M. U. Wehner, H. Kalt, M. Wegener, K. Ohkawa, D. Hommel, and V. M. Axt, Phys. Rev. B **60**, 12 079 (1999).
[48] A. Vagov, V. M. Axt, and T. Kuhn, Phys. Rev. B **66**, 165312 (2002).
[49] L. Allen and J. H. Eberly, *Optical Resonance and Two-Level Atoms* (Wiley, New York, 1975).
[50] G. D. Mahan, *Many-Particle Physics*, 2nd ed. (Plenum, New York, 1990).
[51] K. Huang and A. Rhys, Proc. R. Soc. London, Ser. A **204**, 406 (1950).
[52] C. B. Duke and G. Mahan, Phys. Rev. **139**, A1965 (1965).
[53] S. Schmitt-Rink, D. A. B. Miller, and D. S. Chemla, Phys. Rev. B **35**, 8113 (1987).
[54] S. Mukamel, *Principles of Nonlinear Optical Spectroscopy* (Oxford University, New York, 1995).